Available online at www.sciencedirect.com
ScienceDirect
Cement and Concrete Research 37 (2007) 1427–1439
Cement and Concrete Research

Modelling elasticity of a hydrating cement paste

Julien Sanahuja [a,b,*], Luc Dormieux [a], Gilles Chanvillard [b]

[a] École Nationale des Ponts et Chaussées, Institut Navier, 6 et 8 avenue Blaise Pascal, 77455 Marne-la-Vallée, France
[b] Lafarge Centre de Recherche, 95 rue du Montmurier, BP 15, 38291 Saint-Quentin Fallavier cedex, France

Received 4 October 2006; accepted 9 July 2007

Abstract

Concrete is a complex multi-scale composite involving multi-physics processes. As it is the only evolving component of concrete, the cement paste has a major influence on the mechanical properties of concrete at early age. This paper focuses on the increase of the elastic properties of a cement paste during its hydration. The homogenization theory for disordered media is used in order to estimate the evolution of the effective elastic moduli of the hydrating paste. The morphological model refers to two types of C-S-H (calcium silicate hydrates, main hydration products of Portland cements) distinguished by many authors: inner products or high density C-S-H build up layers surrounding the anhydrous particles, while the outer products or low density C-S-H play the role of a porous matrix.

The simulations of the effective Young's modulus at late age during hydration and at the end of hydration prove to be in excellent agreement with the experimental results available in the literature.

Keywords: Elastic moduli; Micromechanics; Cement paste; Microstructure; Hydration

1. Introduction

1.1. Aim of the paper

During the hydration reaction of cement, hydrates make bonds between dissolving clinker grains and the porosity is progressively reduced. Setting, which corresponds to the achievement of a continuous solid phase, and the progressive increase of the stiffness of the cement paste which follows setting are the focus of the present paper.

Mechanical properties of cement paste at early age have been investigated in several comprehensive experimental studies [1,2] providing measurements of the strength and the stiffness of cement pastes at the macroscopic scale. FEM numerical simulations have been successful in modelling stiffness increase at rather late age. The CEMHYD3D hydration model [3] was used to provide the FEM code with 3D digital images of the microstructure. Still, such a numerical approach requires heavy computational means, so that the classical techniques of the homogenization theory represent an attractive alternative. The present paper aims at evaluating whether such a micromechanics approach coupled with a hydration model is able to yield some realistic prediction of early aged cement paste behavior. Powers hydration model [4] is chosen in the sequel for the sake of simplicity.

In fact, the homogenization theory of disordered media has already been implemented for modelling the early-age poro-elastic characteristics of cement pastes, mortars and concretes [5–7]. At the lowest scale considered in these approaches, a high density stiff C-S-H phase is introduced as an inclusionary constituent with respect to a low density, softer, C-S-H matrix. This heterogeneous material is homogenized and, in a next step, is regarded as a matrix embedding various inclusions such as portlandite or remaining parts of anhydrous (clinker) grains. As compared to these pioneering attempts, the purpose of the present paper is to develop a morphological model distinguishing at the paste scale the so-called inner and outer products, while taking advantage of recent advances concerning nanoscale observation of hydrating clinker grains [8,9].

The model therefore assumes that hydrates precipitate both around anhydrous grains and in the water-filled space. It

* Corresponding author. École Nationale des Ponts et Chaussées, Institut Navier 6 et 8 avenue Blaise Pascal, 77455 Marne-la-Vallée, France.
E-mail addresses: julien.sanahuja@lafarge.com (J. Sanahuja), dormieux@lmsgc.enpc.fr (L. Dormieux), gilles.chanvillard@lafarge.com (G. Chanvillard).

0008-8846/$ - see front matter © 2007 Elsevier Ltd. All rights reserved.
doi:10.1016/j.cemconres.2007.07.003

thus refers to the classical notion of inner and outer products. Anhydrous grains surrounded by a layer of "inner" phase are embedded in an "outer" matrix. At the lower scale, both inner and outer are porous materials made up of the same solid, but with different morphologies and porosities. Setting is controlled by the fluid-to-solid transition of the "outer" matrix.

The model is developed in Section 2. The predictions of the latter are then compared to experimental data: degree of hydration at setting (Section 3.1), increase of Young's modulus during hydration (Section 3.2), Young's modulus at the end of hydration (Section 3.3), and early age Young's modulus obtained by ultra-sonic measurements (Section 3.4).

1.2. Notations

$\underline{a}$	First-order tensor
$\boldsymbol{A}$	Second-order tensor
$\mathbb{A}$	Fourth-order tensor
$\mathcal{T}_1 \otimes \mathcal{T}_2$	Tensorial product of the tensors $\mathcal{T}_1$ and $\mathcal{T}_2$
$\mathcal{T}_1 \cdot \mathcal{T}_2$	Contraction of the tensors $\mathcal{T}_1$ and $\mathcal{T}_2$
$\mathcal{T}_1 : \mathcal{T}_2$	Double contraction of the tensors $\mathcal{T}_1$ and $\mathcal{T}_2$
$\mathcal{T}^{-1}$	Inverse of the tensor $\mathcal{T}$
$\mathbf{1}$	Second-order unit tensor
$\mathbb{I}$	Fourth-order unit tensor
$\mathbb{J}$	Projector extracting the spherical part of a second-order tensor ($\mathbb{J} = 1/3\mathbf{1} \otimes \mathbf{1}$)
$\mathbb{K}$	Projector extracting the spherical part of a second-order tensor ($\mathbb{K} = \mathbb{I} - \mathbb{J}$)

j being a particular phase of the REV:

f_j	Volume fraction of phase j
$\langle a \rangle_j$	Average of the field a over the domain occupied by phase j
$\mathbb{C}_j$	Stiffness tensor of phase j

if phase j is isotropic, $\mathbb{C}_j = 3k_j\mathbb{J} + 2g_j\mathbb{K}$:

k_j	Bulk modulus of phase j
g_j	Shear modulus of phase j
E_j	Young's modulus of phase j
v_j	Poisson's ratio of phase j

with the classical relations: $k_j = \frac{E_j}{3(1-2v_j)}$, $g_j = \frac{E_j}{2(1+v_j)}$, $E_j = \frac{9k_jg_j}{3k_j+g_j}$ and $v_j = \frac{3k_j-2g_j}{6k_j+2g_j}$

usual cement's chemistry abbreviations:

C	CaO
S	SiO_2
H	H_2O

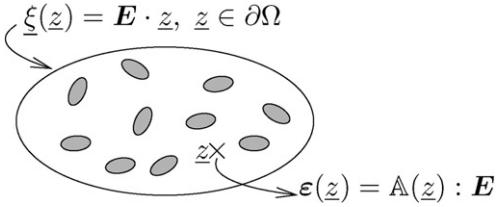

Fig. 2. A schematic REV subjected to uniform strain boundary conditions.

1.3. Principle of homogenization in linear elasticity

This subsection only provides a very brief introduction to micromechanics and homogenization in linear elasticity. To get a detailed presentation, see for example [10].

The homogenization theory aims at estimating the effective behavior of a composite material. This effective behavior can then be used to perform computations at the scale of the structure (Fig. 1). A representative elementary volume (REV) of size l needs to be defined according to two conditions:

- to be elementary, it needs to be small enough compared to the size L of the structure;
- to be representative, it needs to be large enough compared to the size d characterizing the heterogeneity of the microstructure.

Thus the so-called condition for scale separation $d \ll l \ll L$ is a necessary condition for the concept of REV to be valid.

In the framework of homogenization of random composite media, applied to linear elasticity [11], with uniform strain boundary conditions (Fig. 2), the homogenized stiffness tensor reads:

$$\mathbb{C}^{\text{hom}} = \sum_{i=1}^{N} f_i \mathbb{C}_i : \langle \mathbb{A}(\underline{z}) \rangle_i \tag{1}$$

where N is the number of different phases, f_i the volume fraction of phase i, $\mathbb{C}_i$ the stiffness tensor of phase i, $\mathbb{A}(\underline{z})$ the strain concentration tensor (defined on Fig. 2) and $\langle a \rangle_i$ the average of the field a over the domain occupied by phase i.

The average of the strain concentration tensor over phase i is estimated through an appropriate homogenization scheme integrating some information on the morphology. In the Eshelby-based approach, the average strain concentration tensor $\langle \mathbb{A} \rangle_i$ is estimated from the uniform strain which establishes in an ellipsoidal inclusion embedded into an infinite medium with stiffness $\mathbb{C}_0$ subjected to uniform strain boundary conditions at infinity of the form $\underline{\xi}(\underline{z}) = \boldsymbol{E}^{\infty} \cdot \underline{z}$. This reference strain $\boldsymbol{E}^{\infty}$ is

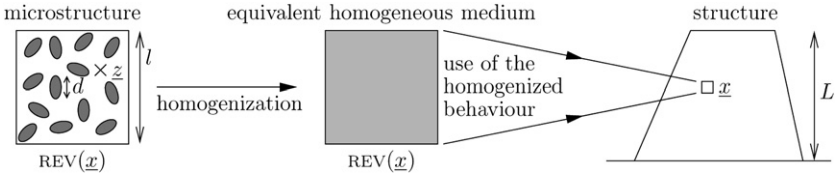

Fig. 1. Principle of homogenization: different length scales.

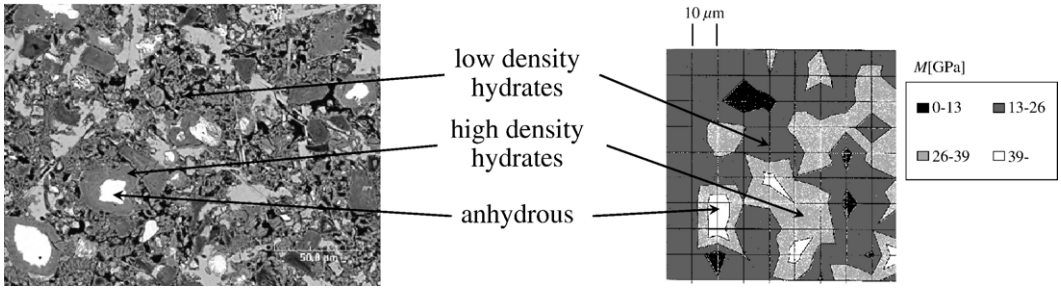

Fig. 3. Polished section and nano-indentation grid [18] on a cement paste at $w/c=0.5$.

related to the strain $\boldsymbol{E}$ applied at the boundary of the REV according to the average strain rule $\langle\varepsilon\rangle=\boldsymbol{E}$. The shape of the ellipsoid representing a given phase and the stiffness $\mathbb{C}_0$ both depend on the morphology of the microstructure. For example, in the self-consistent scheme [12,13], the searched homogenized stiffness tensor is used as the reference stiffness: $\mathbb{C}_0=\mathbb{C}^{\text{hom}}$. The self-consistent scheme is classically used to model polycrystal-like microstructures. When a continuous phase surrounding all the other phases exists (matrix), the Mori Tanaka scheme [14] uses it as the reference medium. The Mori Tanaka scheme takes into account the interactions between the inclusions using the average strain in the matrix as the reference strain $\boldsymbol{E}^{\infty}$.

2. Modelling

2.1. Morphological observations

To estimate the effective elastic moduli of a hydrating cement paste through homogenization of random media, we need to develop a homogenization scheme of such a material. Thus, it is necessary to gather information on the morphology of the cement paste. We use results from various observation techniques at the paste scale and at the hydrates scale.

2.1.1. Polished sections

Several phases are revealed by observation of a polished section of cement paste (left part of Fig. 3):

- white areas: remaining anhydrous grains;
- gray areas around white ones: “high density” hydrates;
- gray and black mixed areas: “low density” hydrates, which seem to be more porous than high density hydrates (black areas being pores);
- light gray areas: portlandite crystals, which are not taken into account in this first approach.

Typical nano-indentation grids (right part of Fig. 3) confirm these morphological observations, suggesting that (1) there is a need for a distinction between two phases in the hydrates, respectively a soft and a stiff one, associated to a low and a high density of solid, and (2) that the high density hydrate phase surrounds the anhydrous phase building up a composite inclusion embedded in the low density hydrate phase.

This argument which is mechanical in nature is confirmed by chemical approaches [15–17] and soft X-ray transmission microscopy observations [8].

2.1.2. Growth of hydrates on an anhydrous grain

The growth of C-S-H on the surface of a C_3S grain wetted by a drop of lime saturated solution has been observed by atomic force microscopy [9,19]. This growth seems to occur by aggregation of small flattened particles of C-S-H whose largest face is parallel to the surface of the grain [9,19]. The size of these particles has been measured: 60 * 30 nm by 5 nm thick. In the sequel, these particles are called “elementary bricks”. We admit that the whole C-S-H part of a cement paste is made up of these elementary bricks, arranged in a way that is discussed in the next section.

2.2. Morphological modelling of a hydrating cement paste

Using the morphological observations from Section 2.1, we now build a homogenization scheme. Fig. 4 schematically represents the morphological model developed in this section.

At the paste scale, composite inclusions (an anhydrous core, denoted by the subscript a, surrounded by a layer called “inner”, denoted by the subscript i) are embedded into a matrix called “outer”, denoted by the subscript o. At a lower scale, both inner and outer are porous media whose solid phase (C-S-H solid, denoted by the subscript s) is made up of the elementary bricks observed in [19]. The two phases only differ by their porosity and morphology. In both inner and outer, the solid phase (respectively the porous phase) is denoted by the superscript s (resp. p).

Inner hydrates are thus considered as a porous polycrystal made up of elementary bricks. Even if the first layers of bricks

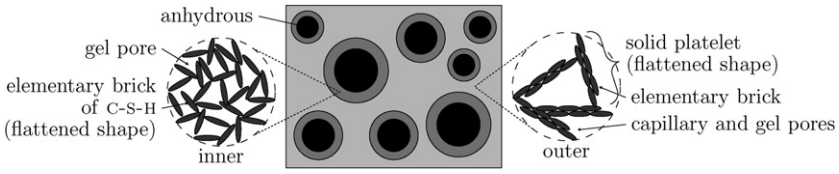

Fig. 4. Schematic representation of the proposed morphological model of cement paste.

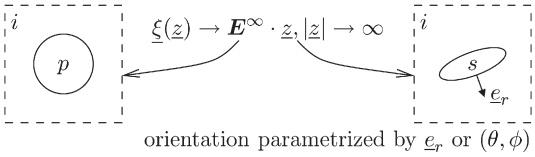

Fig. 5. Schematic representation of the self-consistent scheme proposed to model the inner hydrates.

seem to be parallel to the surface of the grain, the next ones can reasonably be considered as much more randomly packed [9]. To simplify, we assume a uniform distribution of orientation of these bricks. Furthermore, we assume that the porosity of inner is uniform and constant. Only the volume fraction of inner in the paste increases during hydration. The size of the bricks being 60 * 30 * 5 nm, the pores (in between the bricks) size approximately ranges from 5 to 60 nm, which roughly corresponds to the gel pores (1 to 50 nm according to [20]).

Outer hydrates contain both gel pores and capillary pores whose size ranges from 50 nm to 20 μm according to [20]. To reach such sizes, particles much larger than the elementary bricks are required. One way to get such particles is to pack some bricks to form platelets. About 4 to 8 bricks are enough to get a size of 250 nm. As hydration proceeds, more and more platelets are precipitating in the space initially filled with water. Thus the low density hydrates porosity evolves with time. However, we assume that the platelets have a unique shape. From a mechanical point of view, the platelets of outer hydrates have the same characteristics as the bricks of inner hydrates.

The homogenization schemes proposed to model the effective elasticity of inner, outer and the paste are now successively described.

2.2.1. Inner

Inner or high-density hydrates are considered as a porous polycrystal whose solid particles are the elementary bricks observed in [19]. The dimensions of the latter are 60 * 30 * 5 nm. These bricks can be modelled as flat spheroids (oblates), whose aspect ratio (ratio between the diameter parallel to the axis of revolution to a diameter perpendicular to the axis of revolution) would be $r_i^s = 5/\sqrt{30*60} \approx 0.12$.

The morphology being random and polycrystalline, it seems natural to resort to a self-consistent scheme to model the effective elasticity of such a porous material. The scheme proposed here differs from the classical self-consistent scheme: the sphere used to model the solid phase is replaced by a set of oblate spheroids whose orientation is random. The ability of such a self-consistent scheme to model porous polycrystals whose crystals shape is far from spherical will be validated on gypsum.

2.2.1.1. Self-consistent scheme with spheroids. The stiffness tensor of the solid particles is supposed to be isotropic and is denoted by $\mathbb{C}_s = 3k_s\mathbb{J} + 2g_s\mathbb{K}$. In the self-consistent scheme implemented for determining $\mathbb{C}_i$ (Fig. 5), the pore space is represented by a spherical inclusion, and the solid phase is represented by a set of oblate spheroids, which differ in orientation. For simplicity, an isotropic orientation distribution is assumed. The spherical coordinates (r, θ, ϕ) and the spherical base ($\underline{e}_r$, $\underline{e}_\theta$, $\underline{e}_\phi$) are used here.

The spherical pore embedded into an infinite medium with stiffness $\mathbb{C}_i$ (left part of Fig. 5) is a particular case of the Eshelby inhomogeneity problem [21]. The strain in the pore is homogeneous:

$$\boldsymbol{\varepsilon}_p = \langle \boldsymbol{\varepsilon} \rangle_p = \mathbb{A}_p : \boldsymbol{E}^{\infty} \text{ with } \mathbb{A}_p = \frac{3k_i + 4g_i}{4g_i}\mathbb{J} + 5\frac{3k_i + 4g_i}{9k_i + 8g_i}\mathbb{K} \tag{2}$$

where k_i and g_i are the bulk and shear moduli of the inner, respectively.

The uniform strain in the solid spheroid whose axis of revolution is parallel to $\underline{e}_r$ (right part of Fig. 5) is also estimated by the solution of the Eshelby inhomogeneity problem [21]:

$$\boldsymbol{\varepsilon}_s(\theta, \phi) = [\mathbb{I} + \mathbb{P}_i(\theta, \phi) : (\mathbb{C}_s - \mathbb{C}_i)]^{-1} : \boldsymbol{E}^{\infty} \tag{3}$$

where $\mathbb{P}_i(\theta,\phi)$ is the Hill tensor of an oblate spheroid whose axis of revolution is parallel to $\underline{e}_r$. It also depends on k_i, g_i and on the aspect ratio r_i^s of the spheroid, the role of which will be discussed into detail in the next paragraph. For a uniform orientation distribution, the average strain over the whole solid phase reads:

$$\langle \boldsymbol{\varepsilon} \rangle_s = \int_{\phi=0}^{2\pi} \int_{\theta=0}^{\pi} \boldsymbol{\varepsilon}_s(\theta, \phi) \frac{\sin\theta}{4\pi} \mathrm{d}\theta \mathrm{d}\phi \tag{4}$$

An isotropic tensor $\mathbb{A}_s$ can then be introduced as:

$$\begin{aligned} \langle \boldsymbol{\varepsilon} \rangle_s &= \mathbb{A}_s : \boldsymbol{E}^{\infty} \text{ with } \mathbb{A}_s \\ &= \int_{\phi=0}^{2\pi} \int_{\theta=0}^{\pi} [\mathbb{I} + \mathbb{P}_i(\theta, \phi) : (\mathbb{C}_s - \mathbb{C}_i)]^{-1} \frac{\sin\theta}{4\pi} \mathrm{d}\theta \mathrm{d}\phi \end{aligned} \tag{5}$$

The reference strain $\boldsymbol{E}^{\infty}$ is related to $\boldsymbol{E}$ using $\langle \boldsymbol{\varepsilon} \rangle = \boldsymbol{E}$, together with (2) and (5):

$$\boldsymbol{E} = \left[\varphi_i \mathbb{A}_p + (1 - \varphi_i)\mathbb{A}_s\right] : \boldsymbol{E}^{\infty} \tag{6}$$

in which φ_i denotes the porosity of inner. The macroscopic stress is $\boldsymbol{\Sigma} = (1 - \varphi_i)\mathbb{C}_s : \langle \boldsymbol{\varepsilon} \rangle_s$. The effective stiffness tensor $\mathbb{C}_i$

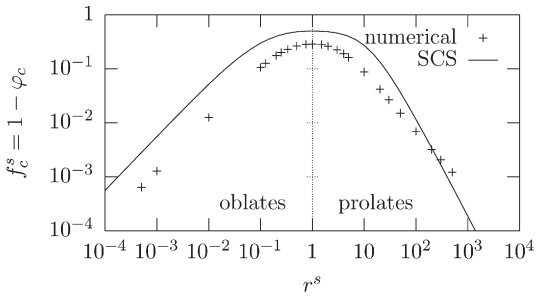

Fig. 6. Critical solid volume fraction as a function of the aspect ratio of the solid particles, estimated by a self-consistent scheme and numerically calculated from geometric considerations (results from [23]).

Table 1
Critical porosity and associated Poisson's ratio for some limit aspect ratios of the solid spheroids

r^s	0	1	∞
φ_c	1	1/2	1
ν_c^{SCS}	≈ 0.173	1/5	$\frac{17-\sqrt{79}}{35} \approx 0.232$

is then defined as the tensor linking the macroscopic strain and stress: $\boldsymbol{\Sigma} = \mathbb{C}_i : \boldsymbol{E}$. Using (5) and (6), the latter reads:

$$\mathbb{C}_i = (1-\varphi_i)\mathbb{C}_s : \mathbb{A}_s : \left[\varphi_i \mathbb{A}_p + (1-\varphi_i)\mathbb{A}_s\right]^{-1} \quad (7)$$

This tensorial equation reduces to two scalar equations since all the tensors involved are isotropic. The self-consistent estimates k_i and g_i of the homogenized bulk and shear moduli are the solutions of these two nonlinear equations.

2.2.1.2. Critical porosity. The standard SCS is generally implemented using a spherical shape for both the solid and the pores, and classically yields a critical porosity $\varphi_c = 1/2$, above which the effective stiffness vanishes. In contrast, when using non spherical spheroids, the critical porosity φ_c proves to depend on the aspect ratio r^s. The latter is defined as the ratio of the length of the symmetry axis over the diameter in the symmetry plane ($r^s > 1$ for prolates, and $r^s < 1$ for oblates). The dependence of φ_c on r^s was already observed for prolates in [22]. The present study confirms this finding for the oblate case. In fact, φ_c only depends on r^s, that is, is not affected by the elastic characteristics of the solid particles.

More precisely, when $r^s \to 1$, corresponding to a spherical shape, the classical value $\varphi_c = 1/2$ is retrieved. The variation of the critical porosity predicted by the SCS as a function of r^s is plotted on Fig. 6 (solid line). The critical solid volume fraction $f_c^s = 1 - \varphi_c$ decreases when the particles are either lengthened or flattened: less solid is needed to reach a given level of stiffness.

Interestingly, the diagram is not symmetrical w.r.t. the axis $r^s = 1$ (for $r^s > 1$, $f_c^s(r^s) < f_c^s(1/r^s)$): intuitively, a network of needles needs less solid to reach the critical solid volume fraction than a network of platelets. As pointed out in [22], the critical porosity disappears ($\varphi_c \to 1$) when $r^s \to \infty$ (Table 1). This is also true when $r^s \to 0$.

Interestingly, Garboczi et al. [23] computed numerical estimates of the geometrical percolation threshold for a network of overlapping spheroids (points on Fig. 6). The fair agreement in terms of critical porosity between the numerical simulations and the self-consistent results supports the use of the latter for investigating the mechanical properties of the hydrates. This is going to be confirmed by experimental data available on gypsum, viewed as a model material of porous polycrystals.

2.2.1.3. Model validation on gypsum. Gypsum is made up of elongated and interlocked crystals [24]. Its microstructure is therefore similar to that of both inner and outer hydrates up to the fact that platelets in the latter are replaced by needles in gypsum. Still, while it is extremely difficult to design samples of pure hydrates, the solid phase in gypsum is homogeneous. It thus seems to be a useful model material for validating a micromechanical modelling based on the self-consistent scheme for polycrystal materials like the hydrates. We hereafter compare the sc scheme results with FEM numerical results and experimental measurements.

We herein refer to FEM simulations of gypsum-like microstructures as reported in [25]. The microstructures were generated by random introduction of 21*3*3 voxels parallelepipeds into a cube. The solid particles have an isotropic linear elastic behavior characterized by $E_s = 45.7$ GPa and $\nu_s = 0.33$.

Fig. 7 left plots the FEM and SCS simulations of the Young's modulus as a function of porosity, together with experimental data [26]. As regards the SCS results (obtained from (7)), the solid particles are represented by prolate spheroids considering three values of the aspect ratio.

Despite the difference in shape between spheroids and parallelepipeds, an excellent agreement is observed, and the consistency with experimental data is reasonable. On low porosities, the SCS results seem to be independent of the aspect ratio, as already observed in [22]. In fact, the latter is found to mainly affect the critical porosity. The curves suggest that an aspect ratio of the order of 15 instead of the aspect ratio of the parallelepipeds should be used to optimize the fit between FEM and SCS simulations.

The agreement between FEM and SCS simulations is confirmed as regards the homogenized Poisson's ratio. The latter is plotted at Fig. 7 right as a function of porosity for three different solid Poisson's ratios, namely 0, 0.2 and 0.33.

2.2.2. Outer

As outer or low density hydrates also have a porous polycrystal-like morphology, with oblate-shaped solid particles,

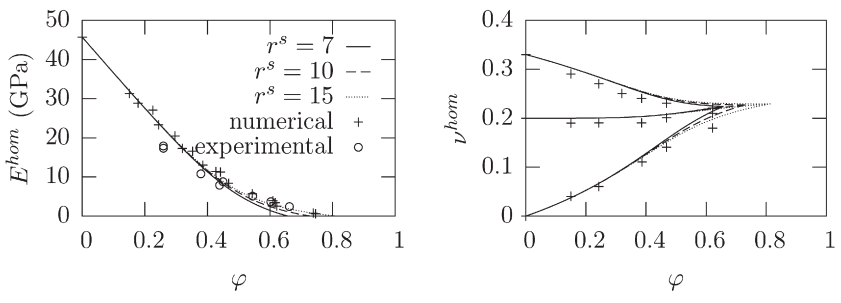

Fig. 7. Young's modulus and Poisson's ratio of a plaster-like microstructure estimated by a self-consistent scheme, numerically calculated (results from [25]) and experimentally measured (from [26]).

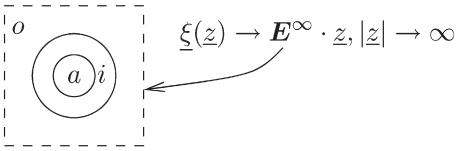

Fig. 8. Schematic representation of the generalized Mori Tanaka scheme proposed to model the paste.

the scheme proposed is exactly the same as the one developed for inner in Section 2.2.1. Only the aspect-ratio r_i^s and the porosity φ_i have to be replaced by their outer equivalents.

2.2.3. Paste

The paste is made up of three phases: anhydrous, inner and outer. To take into account the inclusion-matrix morphology, a generalized Mori Tanaka scheme is proposed (Fig. 8), in the sense of morphologically representative patterns [27].

Fig. 8 depicts a generalized Eshelby problem, where a composite sphere is embedded into an infinite medium of stiffness $\mathbb{C}_o$. Using the approach detailed in [28], this problem is solved successively considering a reference strain $\boldsymbol{E}^{\infty}$ spherical and deviatoric. Contrary to the classical Eshelby problem, the strains in the phases a and i are not homogeneous. The average strains in the anhydrous and inner phases can be written as:

$$\langle \boldsymbol{\varepsilon} \rangle_a = \mathbb{A}_a : \boldsymbol{E}^{\infty} \text{ and } \langle \boldsymbol{\varepsilon} \rangle_i = \mathbb{A}_i : \boldsymbol{E}^{\infty} \tag{8}$$

The Mori Tanaka scheme considers the reference strain $\boldsymbol{E}^{\infty}$ as the average strain in the matrix o:

$$\langle \boldsymbol{\varepsilon} \rangle_o = \boldsymbol{E}^{\infty} \tag{9}$$

The Mori Tanaka estimate of the homogenized paste stiffness tensor then reads:

$$\begin{aligned} \mathbb{C}_{\text{paste}} = &[f_a \mathbb{C}_a : \mathbb{A}_a + f_i \mathbb{C}_i : \mathbb{A}_i + (1 - f_a - f_i)\mathbb{C}_o] \\ &: [f_a \mathbb{A}_a + f_i \mathbb{A}_i + (1 - f_a - f_i)\mathbb{I}]^{-1} \end{aligned} \tag{10}$$

An alternative approach to this generalized Mori Tanaka scheme consists in resorting to an n-layered inclusion-based model [28], which is often used to model inclusion-matrix morphologies. The discrepancy between the Young's modulus of the paste estimated through these two schemes is found to be negligible. This means the generalized Mori Tanaka scheme, being simpler to implement, is also here completely relevant.

2.3. Input data

The homogenization scheme needs as input data the volume fractions and the elastic characteristics of the phases.

2.3.1. Volume fractions

The homogenization scheme developed in the previous section needs as inputs the volume fractions of the five phases involved in the paste model as a two-scales porous composite material: anhydrous (f_a), solid part of inner (f_i^s), porous part of inner (f_i^p), solid part of outer (f_o^s), porous part of outer (f_o^p).

2.3.1.1. Powers model. Although it was already introduced in the 40s, the Powers hydration model [4] has approved to be still relevant and remains widely used because of the easiness of its implementation. It provides the volume fractions of anhydrous (subscript a), hydrates (h) and water (w) as simple functions of the water to cement w/c mass ratio and of the degree of hydration α (volume of hydrated clinker over volume of initial clinker). The required information are the volume of hydrates κ_h created and the volume of water κ_w consumed when a unit volume of anhydrous cement is hydrated, which are stoichiometric characteristics. Denoting the density of anhydrous cement by ρ_a, we have:

$$f_a = \frac{(1-\alpha)}{1+\rho_a w/c},\ f_h = \frac{\kappa_h \alpha}{1+\rho_a w/c} \text{ and } f_w = \frac{\rho_a w/c - \kappa_w \alpha}{1+\rho_a w/c} \tag{11}$$

The Powers model is a numerical implementation of these relations, with ρ_a=3.13, κ_h=2.13 and κ_w=1.31:

$$\begin{aligned} f_a &= \frac{0.32(1-\alpha)}{w/c+0.32}, \\ f_h &= \frac{0.68\alpha}{w/c+0.32} \text{ and } f_w = \frac{w/c - 0.4175\alpha}{w/c+0.32} \end{aligned} \tag{12}$$

The pore space of a cement paste is made up of capillary pores, whose volume fraction is $1–f_a–f_h$, and of gel pores, which are smaller. The volume fraction of the latter is also estimated by the Powers model, so that the total porosity of the paste reads:

$$f_p = \frac{w/c - 0.17\alpha}{w/c+0.32} \tag{13}$$

The evolutions of anhydrous, hydrates and capillary pores volume fractions for w/c=0.3 and 0.5 are depicted at Fig. 9. The

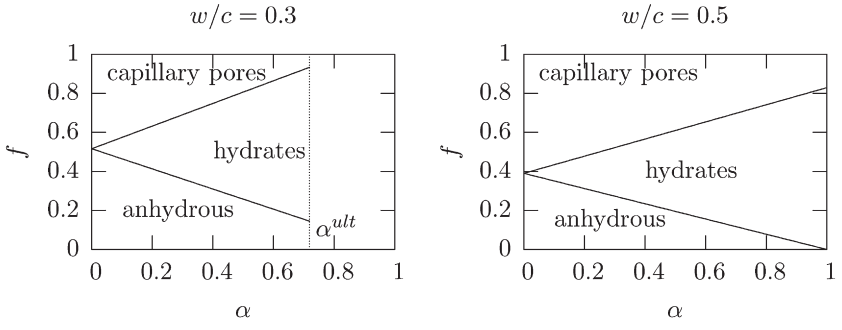

Fig. 9. Volume repartition of anhydrous, hydrates and capillary pores estimated by the Powers model as a function of the degree of hydration.

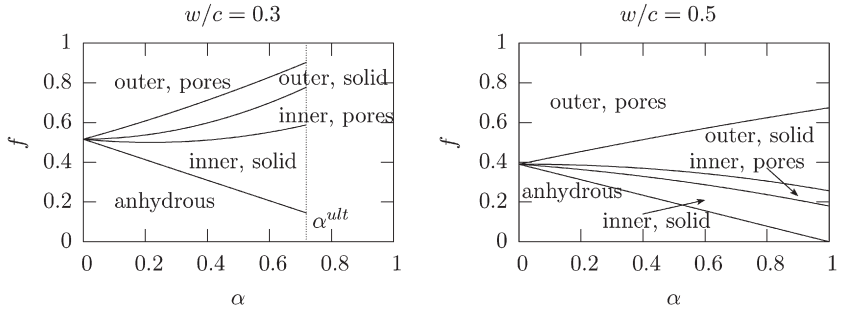

Fig. 10. Volume repartition of the five phases constituting the cement paste (φ_i=0.30).

hydration reaction is assumed to stop at $\alpha=\alpha^{ult}$ when one of the two reactants is depleted. According to *w/c*, this corresponds to $f_a=0$ or $f_w=0$, hence:

$$\alpha^{\text{ult}} = \begin{cases} 1 & \text{if } w/c > \kappa_w/\rho_a \\ \dfrac{w/c}{\kappa_w/\rho_a} & \text{if } w/c < \kappa_w/\rho_a \end{cases} \tag{14}$$

At *w/c*=0.3, hydration stops at $\alpha<1$, because water is depleted: some clinker grains still remain unhydrated (heterogeneous solid phase). At *w/c*=0.5, hydration stops at $\alpha=1$, because anhydrous is depleted: accordingly, the solid phase is homogeneous.

The degree of hydration proves to be more relevant than time for describing the evolution of the hydration state. Indeed, different cement pastes may reach similar morphologies at different times, but these times may correspond to similar degrees of hydration. Nevertheless, the degree of hydration α can be linked to time by means of a hydration kinetics model.

2.3.1.2. Distinction of the two hydrate types. Tennis and Jennings [15] proposed a quantitative model of the distribution of C-S-H into each type, low density (outer) and high density (inner). Their estimate of the ratio of the mass of low density to the total mass of C-S-H reads, in dried conditions:

$$m_{\text{LD}} = 3.017\alpha w/c - 1.347\alpha + 0.538 \tag{15}$$

As the solid part of both types of C-S-H is assumed to have the same density, the mass fraction directly translates into a volume fraction:

$$\frac{f_o^s}{f_o^s + f_i^s} = m_{\text{LD}} \tag{16}$$

2.3.1.3. Volume fractions of the five phases. We are trying to estimate the volume fractions of the five phases making up the cement paste morphological model: anhydrous (f_a), solid part of inner (f_i^s), porous part of inner (f_i^p), solid part of outer (f_o^s), porous part of outer (f_o^p). We thus need to write five relations between these volume fractions. Eq. (16) makes the first one. Two more equations can be obtained writing the total porosity and the total hydrate solid volume fraction:

$$f_i^p + f_o^p = f_p \tag{17}$$

$$f_i^s + f_o^s = f_h^s = 1 - f_a - f_p \tag{18}$$

The anhydrous volume fraction is given by the Powers model (12):

$$f_a = \frac{0.32(1-\alpha)}{w/c + 0.32} \tag{19}$$

A last equation is required. The inner porosity φ_i is supposed to be known and independent of both *w/c* and α (see Section 2.2):

$$\frac{f_i^p}{f_i^P + f_i^s} = \varphi_i \tag{20}$$

The five Eqs. (16), (17), (18), (19) and (20) then allow to derive the volume fractions $f_a, f_i^s, f_i^p, f_o^s, f_o^p$ as functions of φ_i, *w/c* and α (Fig. 10). Finally, the quantities needed by the homogenization scheme can be derived as:

$$f_i = f_i^s + f_i^p \text{ and } \varphi_o = \frac{f_o^p}{f_o^p + f_o^s} \tag{21}$$

Table 2
Mechanical threshold of a cement paste estimated on strength measurements [1]

w/c	α_0^{exp}
0.157	0.07
0.25	0.16
0.35	0.24
0.5	0.25

2.3.2. Elastic characteristics of the different phases

We have already commented on the fact that a hydration model is necessary for predicting the volume fraction of the different mechanical phases involved in the model. Clearly enough, the implementation of the morphological model also requires fundamental elastic characteristics.

The characteristics of the anhydrous phase have been measured by nano-indentation [29] on C_3S: E_a=135 GPa and ν_a=0.3. The elastic constants of the inner phase surrounding the anhydrous cores are also determined from nano-indentation tests as E_i=31 GPa and ν_i=0.24 [30].

As far as the outer phase is concerned, its effective elastic characteristics evolve with time, that is, are function of the degree of hydration α. Therefore nano-indentation techniques can only provide a snapshot of the outer stiffness. This is why a

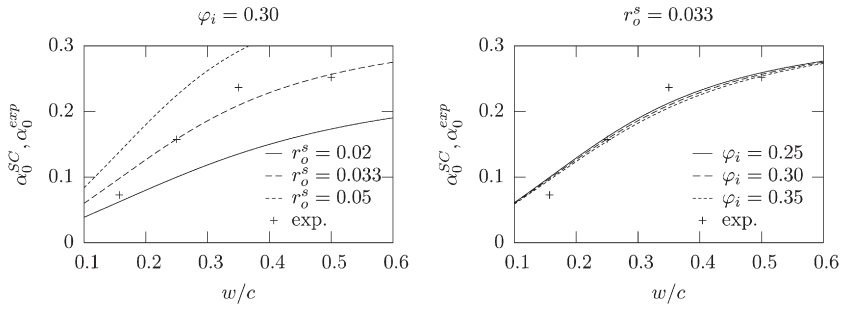

Fig. 11. Degree of hydration at setting estimated by SC scheme, and experimental values from [1].

homogenization estimate of the latter must be derived from Eq. (7). The effective elastic characteristics of the outer also depend on the stiffness of the elementary bricks. These bricks are unfortunately too small to perform nano-indentation measurements.

However, the elastic characteristics of the elementary bricks can be assessed by an inverse analysis of the inner stiffness, as the latter is constant and uniform, and has been measured by nano-indentation (E_i=31 GPa and ν_i=0.24 [30]). The elastic moduli k_i and μ_i calculated from (7) depend on the elastic moduli k_s and μ_s of the bricks, the aspect ratio r_i^s of the bricks and the porosity φ_i of inner. The aspect ratio $r_i^s \approx 0.12$ has been determined in Section 2.2.1 from the size of the bricks. As far as the porosity is concerned, Tennis and Jennings [15] proposed 0.35 and 0.30 using density considerations. Note that the classical value φ_i=0.28 of the so-called gel porosity has been early proposed in the Powers model. The intermediate estimate φ_i=0.3 is used in the sequel which will assess the sensitivity of the simulations to this parameter. Inverse analysis of the elastic moduli of the inner then yields E_s=71.6 GPa and ν_s=0.27.

3. Implementation and experimental validation

The last parameter which remains to be discussed is the aspect ratio r_o^s of the platelets making the outer hydrates. The simulations reported on Figs. 6 and 7 emphasize the fact that the aspect ratio mainly affects the critical porosity φ_c associated with the onset of the effective stiffness. There is therefore good hope that the optimal aspect ratio can be derived from experimental data concerning the setting degree of hydration.

3.1. Calibration of the aspect ratio of the platelets

Using Taplin's experiments on strength of cement pastes [31], quoted by Byfors [32], Torrenti and Benboudjema [1] defined a threshold α_0^{exp} of the degree of hydration, below which the strength of the paste can be neglected. More precisely, Torrenti and Benboudjema assumed an affine relationship between the compressive strength and the degree of hydration: $\sigma_c = \sigma_c^0(\alpha - \alpha_0^{exp})$. Then, they estimated α_0^{exp} by affine regression on experimental data (α, σ_c) available for some values of w/c (see Table 2). We should mention that α_0^{exp} only represents an estimate of the degree of hydration at setting. In particular, some experimental points ($\alpha < \alpha_0^{exp}$, $\sigma_c > 0$) exist, showing that a paste hydrated at $\alpha < \alpha_0^{exp}$ can exhibit some (small) compressive strength. In other words, α_0^{exp} represents a degree of hydration at setting which neglects the beginning of the (α, σ_c) curve corresponding to very early age.

The onset of stiffness at the scale of the cement paste occurs when the critical solid volume fraction is reached in the outer phase. The porosity of the outer is given by (21), which reads formally $\varphi_o = \Phi(w/c, \alpha)$. The self-consistent estimate α_0^{SC} (w/c) of the setting degree of hydration is therefore the solution to the equation $\varphi_c(r_o^s) = \Phi(w/c, \alpha_0^{SC}(w/c))$, where the function $\varphi_c(r_o^s)$ can be derived from Fig. 6. The aspect ratio r_o^s has to be optimized so as to minimize the distance between the experimental results $\alpha_0^{exp}(w/c)$ and the SC estimate α_0^{SC} (w/c).

The optimum value of the aspect ratio of the platelets is found to be r_o^s=0.033 (see left part of Fig. 11). The setting degree of hydration hardly depends on φ_i in the range 0.25–0.35 (Fig. 11 right). This justifies the arbitrary choice φ_i=0.30.

The optimal value of the aspect ratio of the platelets r_o^s=0.033 differs from the aspect ratio of the elementary bricks r_i^s=0.12. This difference justifies the idea of platelet introduced for the outer hydrates, which can be defined as the juxtaposition of several elementary bricks.

3.2. Evolution of Young's modulus during hydration

Table 3 summarizes the parameters used for the implementation of the model.

Haecker et al. [2] measured the degree of hydration and Young's modulus at 14, 28 and 56 days on two different cements for w/c ranging from 0.25 to 0.6.

Fig. 12 plots together experimental data and the model predictions. The agreement is very satisfactory on the whole range of w/c ratios. It is emphasized that the simulations are based on mechanical and morphological parameters taken from

Table 3
Input data used in simulations

	E (GPa)	ν
Anhydrous (a)	135	0.3
Inner (i)	31	0.24
Hydrate solid (s)	71.6	0.27
r_i^s	0.12	
r_o^s	0.033	
φ_i	0.30	

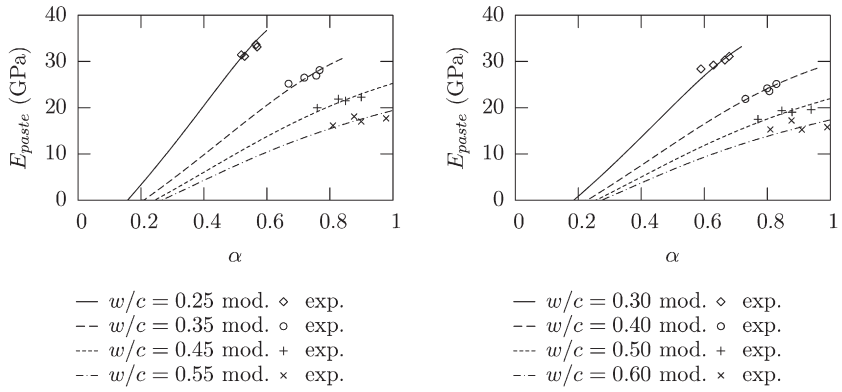

Fig. 12. Young's modulus of paste estimated by model, and experimental values from [2].

the literature, except for the aspect ratio of the platelets which has been calibrated in order to predict correctly the experimental setting degree of hydration. It is all the more interesting to note that the range of degree of hydration covered by the experimental data of Fig. 12 corresponds to an advanced stage of hydration far from setting.

The evolution of the outer Young's modulus E_o as a function of the degree of hydration is plotted on Fig. 13. As expected, E_o is an increasing function of the degree of hydration, and is higher for lower w/c ratios. Interestingly, the asymptotic values (at $\alpha=\alpha^{ult}$ according to (14)) are not so far from the nano-indentation results on low density hydrates reported in [30] (20±2 GPa).

3.3. Young's modulus of fully hydrated pastes

Let us leave the field of early aged pastes and move to the one of hardened pastes. The model predictions are still based on the input data gathered in Table 3. The degree of hydration of the pastes that are considered now is assumed to correspond to the ultimate state predicted by the Powers model, reached when one of the two reactants is depleted, see (14).

Experimental data of comparison are taken from Helmuth and Turk [33] who used three different materials: two portland cements and a nearly pure C_3S. The Young's modulus was deduced from measurements of the fundamental flexural and torsional resonance frequencies of thin slabs specimens with w/c from 0.3 to 0.6. C_3S samples were aged 8 and 14 months at testing, and portland cement samples were aged 6, 7, 8, 14 and 24 months.

The curve (see Fig. 14) exhibits an angular point at $w/c=\kappa_w/\rho_a$ ($\approx$0.42) which corresponds to the transition from a three phases composite (anhydrous, hydrates and pores) to a two phases one (hydrates and pores). Indeed, in the ultimate state, all the anhydrous phase has reacted for $w/c>\kappa_w/\rho_a$ whereas some anhydrous cores remain for $w/c<\kappa_w/\rho_a$.

The fact that the experimental stiffness is underestimated around $w/c=0.3$ could possibly be due to an underestimation of the real degree of hydration: some additional water might have penetrated the sample to conduct hydration a little further. Generally speaking, the discrepancy between experimental and theoretical results is acceptable.

3.4. Young's modulus at early age

Experimental data used in Section 3.2 concerned rather aged pastes (more than 14 days). Indeed, standard mechanical tests on very early age pastes are difficult to perform.

Boumiz [34] did ultra-sonic measurements of the elasticity of C_3S and white cement pastes at early age. The ultra-sonic technique allowed to start measurements nearly from $\alpha=0$. The pastes being saturated with water, the elastic moduli obtained are the undrained ones. Indeed, classical poromechanics [35] define two extreme cases for the elastic stiffness tensor of a saturated porous medium:

- drained stiffness, when the pressure in the pores is vanishing;
- undrained stiffness, in the absence of fluid mass exchange with the outside.

Until now, the model has focused on the drained stiffness. Some work needs to be done to obtain the undrained stiffness required to compare the micromechanical estimates to the ultrasonic measurements.

3.4.1. Undrained elastic moduli

The relation between the effective drained ($\mathbb{C}_{hom}$) and undrained ($\mathbb{C}^u_{hom}$) stiffness of a saturated porous medium is [10]:

$$\mathbb{C}^u_{hom} = \mathbb{C}_{hom} + M\boldsymbol{B}\otimes\boldsymbol{B} \tag{22}$$

where $\boldsymbol{B}$ is the tensorial Biot coefficient and M is the Biot modulus of the whole porous material. When the material is

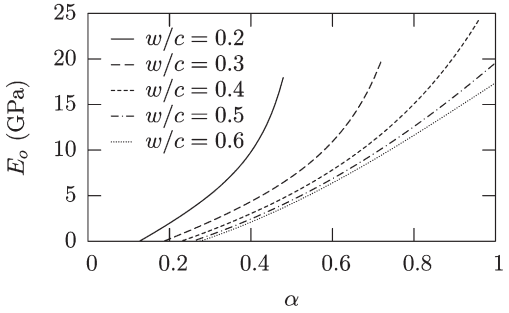

Fig. 13. Estimated Young's modulus of the outer, for various w/c.

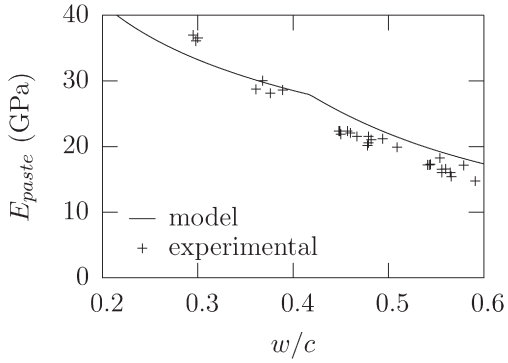

Fig. 14. Young's modulus of fully hydrated pastes estimated by model and experimental values from [33].

macroscopically isotropic, this translates in terms of bulk and shear moduli:

$$k^u_{\text{hom}} = k_{\text{hom}} + \text{Mb}^2 \text{ and } \mu^u_{\text{hom}} = \mu_{\text{hom}} \tag{23}$$

where b is the Biot coefficient ($\boldsymbol{B}=b\boldsymbol{1}$). When, furthermore, the solid phase is homogeneous and isotropic (bulk and shear moduli being denoted by k_s and μ_s), the Biot coefficient and the Biot modulus of the whole porous material read [10]:

$$b = 1 - \frac{k_{\text{hom}}}{k_s} \text{ and } M = \frac{k_s}{b-\varphi} \tag{24}$$

As inner and outer are isotropic porous media whose solid phase is homogeneous and isotropic, their undrained moduli can be easily calculated from the drained ones (see Sections 2.2.1 and 2.2.2) using (23) and (24).

As far as the paste is concerned, its moduli in undrained conditions are estimated as described in Section 2.2.3, replacing the drained moduli of inner and outer by the undrained ones.

3.4.2. Comparison

Fig. 15 left plots together experimental data and model predictions, still obtained from input data summarized in Table 3. The agreement is not so good, especially at very early age ($\alpha<0.3$). It can be quantified by the root mean square (RMS) error. The latter is defined by:

Table 4
Optimization of the aspect ratio of the outer solid platelets

w/c	r^s_o opt.	RMS error (GPa)
0.3	0.015	1.56
0.4	0.028	1.31
0.5	0.033	1.28
0.6	0.035	0.96

$$\text{RMS error} = \sqrt{\frac{\sum_{i=1}^{n} \left(E_i^{exp} - E_i^{\text{mod}}\right)^2}{n}} \tag{25}$$

where n is the number of experimental points, E_i^{exp} and E_i^{mod} are respectively the experimental and modelled Young's modulus at point $i=1..n$. The RMS error is 2.36 GPa. The present model needs some improvements at early age. Moreover, the setting degree of hydration obtained by ultra-sonic measurements is very different from the one used in Section 3.1. Thus, we can try to recalculate the optimal aspect ratio r^s_o of the outer platelets, minimizing the RMS error between the ultrasonic experimental data and the model predictions. Doing such an optimization on a per-w/c basis yields the results listed in Table 4. This improves a bit the agreement between the experimental data and the model predictions, as shown on Fig. 15 right.

3.4.3. Validity of the model of outer at early age

The optimization of the aspect ratio of the outer solid platelets did not provide accurate predictions of the ultra-sonic measurements of the setting degree of hydration. We now also consider the influence of the ratio m_{LD} characterizing the distribution of C-S-H between outer and inner products. The self-consistent estimate α_0^{SC} of the setting degree of hydration determined in Section 3.1 can be calculated as a function of m_{LD}, without introducing the expression (15) proposed by [15].

Fig. 16 plots α_0^{SC} as a function of m_{LD} for a few values of the w/c ratio and the aspect ratio r^s_o of the outer solid platelets. An aspect ratio below 0.02 might not be so realistic since a platelet would need a juxtaposition of at least 0.12/0.02=6 elementary

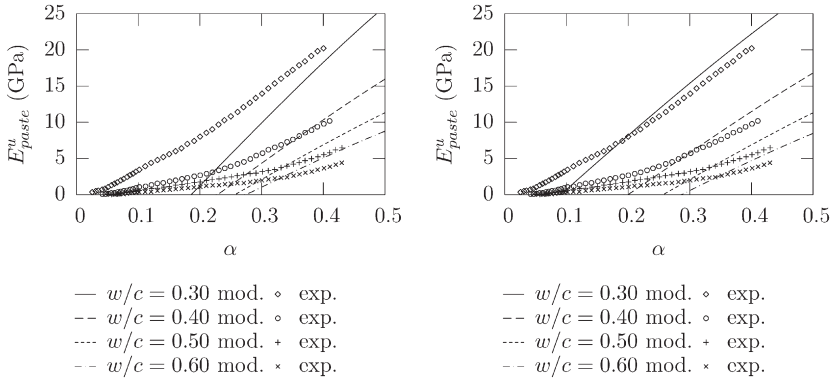

Fig. 15. Undrained Young's modulus of paste estimated by model, and experimental ultra-sonic measurements [34] (left: $r^s_o=0.033$; right: r^s_o optimized on a per-w/c basis).

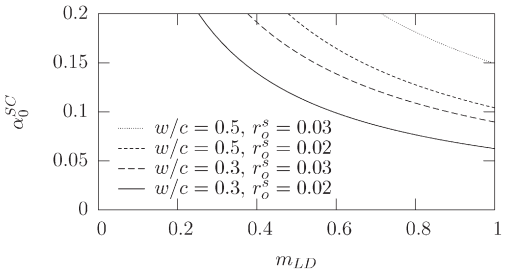

Fig. 16. Self-consistent estimate of the setting degree of hydration as a function of the ratio between outer and inner products (φ_i=0.3).

bricks to be formed (0.12 being the aspect ratio of the elementary brick). The ratio m_{LD} is obviously restricted to the range [0,1]. The experimental setting degree of hydration determined from Fig. 15 is <0.03 for w/c=0.3 and <0.1 for w/c=0.5. Clearly enough, no value of m_{LD} would allow to reach such setting degrees of hydration (see Fig. 16). This means that the morphological model of the outer hydrates viewed as a porous foam needs some refinements at early age.

3.5. Improved model of outer

The comparison of model predictions to ultra-sonic measurements from [34] in subsection 3.4 revealed that the outer model needs some refinements at least at early age. In order to reproduce the degree of hydration at setting estimated from the ultra-sonic measurements, it was necessary to resort to an unrealistically small platelet aspect ratio.

The main criticism which can be formulated against the present model lies in the fact that the solid phase of the outer is uniformly distributed in the space in between the composite anhydrous+inner spheres. This yields a very low density of the outer described as a porous foam. Simultaneously, the model fails to take into account the well accepted description of the capillary pores (at least, the largest ones) as a reminiscence of the complementary space with respect to the clinker particles. Clearly, a more accurate geometrical representation of the outer is due.

The idea is to keep the matrix concept embedding the composite anhydrous+inner spheres, but now, this matrix is regarded as a double porosity material. It is made up of the outer phase itself, still described as a porous foam, and of the largest capillary pores. The typical size of the latter is of the order of 10 μm, while the platelets (packs of a couple of elementary 60*30*5 nm bricks) making up the foam are of the order of 100 nm. This scale separation justifies to represent the matrix as a porous material which "solid" phase is the homogenized porous foam, that is, the outer (see Fig. 17).

From a technical point of view, the mechanical properties of this matrix can be estimated by two successive self-consistent schemes:

- platelets and small pores are homogenized to build up the outer (porous foam), using the self-consistent scheme already implemented to model inner and the previous outer (see Section 2.2.1);
- the outer and large pores are homogenized to build up the matrix, using a classical self-consistent scheme with spherical shapes (see for example [10] p.193).

For technical purposes, it is convenient to introduce the volume fraction f_m of the matrix, which is the sum of the contribution of the solid (f_m^s) and that of the matrix pore space (f_m^p). With the notations introduced in Section 2.3.1, it is emphasized that f_m, f_m^s *and* f_m^p respectively replace the previous quantities f_o, f_o^s *and* f_o^p. The matrix porosity reads $\varphi_m = f_m^p/f_m$.

The description of the matrix pore space refers to two well separated sizes of pores. On the one hand, we find the largest capillary pores (up to 20 μm). They make up the pore phase in the second homogenization step (foam+pore space). On the other hand, the porous foam (outer) comprises the smallest capillary pores (up to 150 nm) and gel pores. The new model therefore introduces an additional scalar morphological parameter χ which splits the matrix porosity φ_m into the largest capillary pores ($(1-\chi)\varphi_m$) and the foam pores ($\chi\varphi_m$). Note that the new model is indeed an extension of the previous one which is retrieved in the case χ=1.

Obviously, the condition that the outer be less dense than the inner introduces some restrictions on χ, stating that the foam porosity be greater than the inner one φ_i:

$$\frac{\chi f_m^p}{\chi f_m^p + f_m^s} > \varphi_i \tag{26}$$

which yields:

$$\chi > \chi_{\min} \frac{\varphi_i}{1-\varphi_i}\left(\frac{f_m}{f_m^p} - 1\right) \tag{27}$$

where $\chi_{\min}$ depends on w/c and α. The latter is plotted as a dotted line on Fig. 18. The part of the (χ, α) plane situated on the left of this dotted line (gray area) should be avoided to ensure (27).

The setting of the paste is controlled by that of the matrix. The latter requires that (i) enough platelets have precipitated in the outer porous foam and that (ii) the porosity of the matrix (in

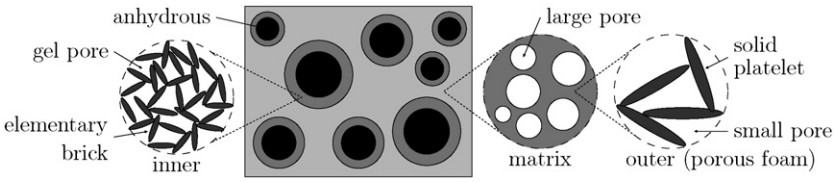

Fig. 17. Schematic representation of the proposed morphological model of cement paste, with the improved model of outer.

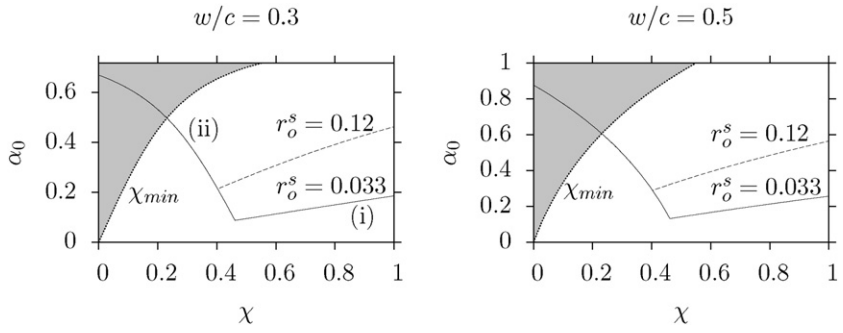

Fig. 18. Degree of hydration at setting as a function of χ, for some w/c and r_o^s; only the part of the graph situated on the right of the dotted line is valid ($\chi > \chi_{min}$).

the second homogenization step) is lower than 1/2: $(1-\chi)f_m^p/f_m < 1/2$. Condition (i) (resp. (ii)) corresponds to the threshold plotted on the right (resp. left) curve at Fig. 18. The degree of hydration at setting of the cement paste thus depends not solely on the w/c ratio and on the aspect ratio r_o^s of the platelets, but also on χ. For illustrative purposes, let us consider values of w/c ranging between 0.3 and 0.5, and the same value $r_o^s = 0.033$ as before. Compared to the previous model (corresponding to $\chi = 1$), it appears that all values of χ in the interval [0.45,1] predict lower degrees of hydration at setting, closer to what ultra-sonic tests suggest [34].

The morphological parameter χ is expected to be a function $\chi(w/c, \alpha)$. Further investigation is definitely necessary in order to clarify the way χ depends on these two parameters. Still, for illustrative purposes, we can propose simulations based on a constant χ, chosen as the minimal one satisfying $\chi > \chi_{min}$ in the range $0.2 < w/c < 0.6$: $\chi = 0.72$. Simulations of the increase of the (drained) Young's modulus of the paste are plotted on Fig. 19, using $\chi = 0.72$ and $\chi = 1$ which corresponds to the previous model. With $\chi = 0.72$, the degree of hydration at setting is reduced, as expected from Fig. 18, and the increase of the Young's modulus is slower at the beginning of hydration. However, later on ($\alpha > 0.4$), the predictions of the new model are nearly equivalent to those of the previous one. This is a good news in so far as a fair agreement had been obtained with the previous model at late age.

4. Conclusion

The model developed in this paper successfully predicts the evolution of the Young's modulus of a cement paste at late age ($\alpha > 0.5$). Some improvements are still necessary at early age ($\alpha < 0.3$). In this respect, a refinement of the basic model has already provided promising improvements. We should mention that two other models have been developed, basically considering only one type of hydrates. More precisely, the first model considers anhydrous particles embedded in a homogeneous foam of hydrates, while the second one deals with a random distribution of capillary pores and composite spheres made up of an anhydrous core surrounded by a homogeneous layer of hydrates. The results of these models in terms of Young's modulus are less satisfactory than those described in the present paper. This is likely to be due to the fact that the microstructure they refer to is not consistent with the existence of two distinct types of hydrates, which seems to be confirmed experimentally, for instance by nano-indentation tests [36].

On the route towards industrial implementation, a number of improvements are necessary, especially at early age. Indeed, the distinction between high and low density hydrates is not sufficient: real cement pastes also comprise various products of hydration which differ not only in terms of density but also on the chemical level. Nevertheless, incorporating new components such as portlandite or aluminates seems to be a straightforward extension of the present model, provided that a more sophisticated hydration model be available. Incorporating portlandite would allow for example to simulate the mechanical effect of calcium leaching, where portlandite progressively dissolves.

The real task which remains to be done consists in dealing with nonlinear phenomena and aging behaviors which are necessary for addressing strength or creep. Owing to recent improvements in advanced homogenization techniques [37,27],

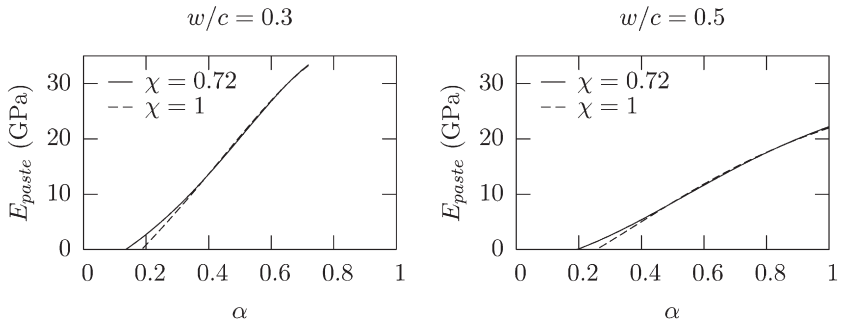

Fig. 19. Young's modulus of paste during hydration.

the main challenge is to characterize the behavior of the constituents at the microscopic scale, beyond the elastic regime. Ongoing researches in this direction are expected to provide in the next future, at least a partial answer to this demand.

Acknowledgements

The authors gratefully acknowledge Dr. N.P. Lociso for fruitful discussions.

References

[1] J.M. Torrenti, F. Benboudjema, Mechanical threshold of cementitious materials at early age, Materials and Structures 38 (2005) 299–304.
[2] C.-J. Haecker, E.J. Garboczi, J.W. Bullard, R.B. Bohn, Z. Sun, S.P. Shah, T. Voigt, Modeling the linear elastic properties of portland cement paste, Cement and Concrete Research 35 (2005) 1948–1960.
[3] D.P. Bentz, Three-dimensional computer simulation of portland cement hydration and microstructure development, Journal of the American Ceramic Society 80 (1997) 3–21.
[4] T.C. Powers, T.L. Brownyard, Studies of the physical properties of hardened portland cement paste (nine parts), Journal of the American Concrete Institution 43 (Oct. 1946 to April 1947).
[5] O. Bernard, F.-J. Ulm, E. Lemarchand, A multiscale micromechanics-hydration model for the early-age elastic properties of cement-based materials, Cement and Concrete Research 33 (2003) 1293–1309.
[6] G. Constantinides, F.-J. Ulm, The effect of two types of C-S-H on the elasticity of cement-based materials: results from nanoindentation and micromechanical modelling, Cement and Concrete Research 34 (2004) 67–80.
[7] F.-J. Ulm, G. Constantinides, F.H. Heukamp, Is concrete a poromechanics material?-a multiscale investigation of poroelastic properties, Materials and Structures 37 (2004) 43–58.
[8] M.C.G. Juenger, V.H.R. Lamour, P.J.M. Monteiro, E.M. Gartner, G.P. Denbeaux, Direct observation of cement hydration by soft X-ray transmission microscopy, Journal of Materials Science Letters 22 (2003) 1335–1337.
[9] S. Garrault-Gauffinet. Étude expérimentale et par simulation numérique de la cinétique de croissance et de la structure des hydrosilicates de calcium, produits d'hydratation des silicates tricalcique et dicalcique. PhD thesis, Université de Bourgogne, 1998.
[10] L. Dormieux, D. Kondo, F.-J. Ulm, Microporomechanics, Wiley, 2006.
[11] A. Zaoui, Continuum micromechanics: survey, Journal of Engineering Mechanics 128 (2002) 808–816.
[12] R. Hill, A self consistent mechanics of composite materials, Journal of the Mechanics and Physics of Solids 13 (1965) 213–222.
[13] B. Budiansky, On the elastic moduli of some heterogeneous materials, Journal of the Mechanics and Physics of Solids 13 (1965) 223–227.
[14] T. Mori, K. Tanaka, Average stress in matrix and average elastic energy of materials with misfitting inclusions, Acta Metallurgica 21 (5) (1973) 1605–1609.
[15] P.D. Tennis, H.M. Jennings, A model for two types of calcium silicate hydrate in the microstructure of portland cement pastes, Cement and Concrete Research 30 (2000) 855–863.
[16] I.G. Richardson, The nature of the hydration products in hardened cement pastes, Cement and Concrete Composites 22 (2000) 97–113.
[17] S. Diamond, The microstructure of cement paste and concrete – a visual primer, Cement and Concrete Composites 26 (2004) 919–933.
[18] G. Constantinides. Invariant mechanical properties of calcium silicate hydrates (C-S-H) in cement-based materials: Instrumented nanoindentation and microporomechanical modelling. PhD thesis, Massachusetts Institute of Technology, 2005.
[19] S. Garrault, E. Finot, E. Lesniewska, A. Nonat, Study of C-S-H growth on C_3S surface during its early hydration, Materials and structures 38 (2005) 435–442.
[20] R.E. Oberholster, Pore structure, permeability and diffusivity of hardened cement paste and concrete in relation to durability: Status and prospects, In 8th International congress on chemistry of cement, 1986, pp. 323–335, Rio de Janeiro.
[21] J.D. Eshelby, The determination of the elastic field of an ellipsoidal inclusion, and related problems, Proceedings of the Royal Society of London. Series A 241 (1957) 376–396.
[22] A. Fritsch, L. Dormieux, C. Hellmich, Porous polycristals built up by uniformly and axisymmetrically oriented needles: Homogenization of elastic properties, C. R. Mecanique 334 (2006) 151–157.
[23] E.J. Garboczi, K.A. Snyder, J.F. Douglas, M.F. Thorpe, Geometrical percolation threshold of overlapping ellipsoids, Physical Review E Online 52 (1) (July 1995) 819–828.
[24] D. Jeulin, P. Monnaie, F. Péronnet, Gypsum morphological analysis and modeling, Cement and Concrete Composites 23 (2001) 299–311.
[25] S. Meille, E.J. Garboczi, Linear elastic properties of 2D and 3D models of porous materials made from elongated objects, Modelling and Simulation in Materials Science and Engineering 9 (2001) 371–390.
[26] S. Meille. Etude du comportement mécanique du plâtre pris en relation avec sa microstructure. PhD thesis, INSA Lyon, 2001.
[27] A. Zaoui, Structural morphology and constitutive behavior of microheterogeneous materials, in: P. Suquet (Ed.), Continuum micromechanics. CISM Courses and Lectures n, vol. 377, Springer, 1997.
[28] É. Hervé, A. Zaoui, n-layered inclusion-based micromechanical modelling, International Journal of Engineering Science 31 (1993) 1–10.
[29] K. Velez, S. Maximilien, D. Damidot, G. Fantozzi, F. Sorrentino, Determination by nanoindentation of elastic modulus and hardness of pure constituents of portland cement clinker, Cement and Concrete Research 31 (4) (2001) 555–561.
[30] P. Acker, Micromechanical analysis of creep and shrinkage mechanisms, in: F.-J. Ulm, Z.P. Bažant, F.H. Wittmann (Eds.), Creep, shrinkage and durability mechanics of concrete and other quasi-brittle materials, proceedings of the sixth international conference CONCREEP6, Elsevier, 2001, pp. 15–25.
[31] J.M. Taplin, A method of following the hydration reaction in portland cement paste, Australian Journal of Applied Science 10 (3) (1959) 329–345.
[32] J. Byfors. Plain concrete at early ages. PhD thesis, Swedish cement and concrete institute, Sweden, 1980.
[33] R.A. Helmuth, D.H. Turk, Elastic moduli of hardened portland cement and tricalcium silicate pastes: effect of porosity, In Symp. Struct. Portland Cem. Paste Concr., 1966, pp. 135–144.
[34] A. Boumiz, D. Sorrentino, C. Vernet, F. Cohen Tenoudji, Modelling the development of the elastic moduli as a function of the degree of hydration of cement pastes and mortars, Second RILEM workshop on hydration and setting, editors, Why does cement set? an interdisciplinary approach, Dijon, France, june 1997.
[35] O. Coussy, Poromechanics, Wiley, 2003.
[36] G. Constantinides, F.-J. Ulm, The nanogranular nature of C-S-H, Journal of the Mechanics and Physics of Solids 55 (2007) 64–90.
[37] P. Suquet, Effective behavior of non linear composites, in: P. Suquet (Ed.), Continuum micromechanics, CISM Courses and Lectures n, vol. 377, Springer, 1997.